J Mater Sci (2011) 46:5423–5431
DOI 10.1007/s10853-011-5483-y

Structural evolution of the intergrowth bismuth-layered $Bi_7Ti_4NbO_{21}$

X. Gao · H. Gu · Y.-X. Li · Z.-G. Yi · M. Čeh · K. Žagar

Received: 10 January 2011 / Accepted: 17 March 2011 / Published online: 1 April 2011

Abstract A series of intergrowth bismuth-layered ferroelectric $Bi_7Ti_4NbO_{21}$ materials are reactive-sintered at 1050 to 1150 °C from Bi_3TiNbO_9 and $Bi_4Ti_3O_{12}$ parent phases to infer their structural characters and microstructure relations. Various types of stacking faults are revealed in the intergrowth structure with extra Bi_3TiNbO_9 or $Bi_4Ti_3O_{12}$ layer(s) by high-resolution transmission electron microscopy; some faults with even spacing form locally new intergrowths of $Bi_{10}Ti_5Nb_2O_{30}$ and $Bi_{11}Ti_7NbO_{33}$. Co-growth of $Bi_7Ti_4NbO_{21}$ epitaxially grown onto the remaining $Bi_4Ti_3O_{12}$ grains is found in the low temperature sintered samples, while the $Bi_4Ti_3O_{12}$ co-growth onto the intergrowth grains is also found in the high temperature samples. Both co-growths are created from intergranular melts during a solution-precipitation process, which is consistent with the anisotropic growth of the intergrowth structure and the presence of a Bi-rich intergranular phase. The populations of different stacking faults are found to decrease with the increase of their thickness and also with the increase of sintering temperature, indicating that they are remnants survived from dissolution to imbed via precipitation into the intergrowth structure, which should be created from the smaller but much abundant one-layered remnants of the parent phases. This leads to a new model of structural reorganization by such one-layered units to form the intergrowth structure in this solution-precipitation process. Such incomplete dissolution is initiated by the preferential melting of interleaved $[Bi_2O_2]^{2+}$ sheets to enable the exfoliation of perovskite layers to re-order into the intergrowth structure. This reorganization model re-defines the reactive sintering as an evolution process of Bismuth-layered structures.

X. Gao · H. Gu (✉) · Y.-X. Li · Z.-G. Yi
State Key Laboratory of High Performance Ceramics and Superfine Microstructures, Shanghai Institute of Ceramics, Chinese Academy of Sciences, Shanghai 200050, China
e-mail: gu@mail.sic.ac.cn

X. Gao
Graduate School Chinese Academy of Science, Beijing 100039, China

M. Čeh · K. Žagar
Department of Nanostructured Materials, Jožef Stefan Institute, Ljubljana 1000, Slovenia

Introduction

The bismuth layer-structured ferroelectrics (BLSF) have attracted increasing attention due to high Curie temperature and fatigue-free ferroelectric properties which makes them suitable candidates for applications in high temperature piezoelectrics and non-volatile ferroelectric random access memories (FeRAM) [1, 2]. These materials have the Aurivillius-type structures with a general formula of $[Bi_2O_2][A_{m-1}B_mO_{3m+1}]$ where m is the number of corner-sharing $[BO_6]$ octahedra that form the pseudo-perovskite blocks separated by the $[Bi_2O_2]^{2+}$ layers [3]. As their crystal chemistry, chemical stability, as well as dielectric and ferroelectric properties of BLSF can be affected by the value of m [4], intergrowth BLSF (*i*BLSF) compounds with two constituent structures (m and $m + 1$) alternating along the common c-axis were synthesized to enable further tailoring of the ferroelectric properties [5–7]. $Bi_7Ti_4NbO_{21}$ (*i*BTN, $m = 2 + 3$) is one such *i*BLSF formed by Bi_3TiNbO_9 (BTN, $m = 2$) and $Bi_4Ti_3O_{12}$ (BiT, $m = 3$) [8]. Consequently, the *i*BLSF compounds have renewed or

expanded structure–property relationship from the parent structures [9–12]. Recently, the spontaneous polarization ($2P_s$) of *i*BTN compound has enhanced to be larger than those of its parent BTN and BiT compounds [13, 14].

Rao et al. proposed that the elastic force created from the structural mismatch governs such ordered intergrowth, since an alternation of two constituent layers corresponds to lower elastic energy as compared with the sum of its parent phases [15, 16]. This model could explain the earlier observations of *i*BTN ($m = 2 + 3$) in alternative stacking of BTN ($m = 2$) and BiT ($m = 3$) layers using high-resolution transmission electron microscopy (HRTEM) [17]. However, the actual stacking in *i*BTN compounds could deviate locally from the perfect order since the "-BTN-BTN-" sequences were found in later observations [18], which may not be readily interpreted by the elastic strain model, unless being regarded as purely a structural fluctuation. In addition, no information concerning the structural changes involved in the phase evolution process was available until now for this intergrowth phase. Therefore, there should be a systematic investigation on the process and mechanism of *i*BTN formation, especially by HRTEM which enables a direct examination of the stacking sequences on the intergrowth layered-structures [17, 19].

In this study, we undertake mainly a TEM analysis of the intergrowth structure in a series of *i*BTN ceramics to reveal detailed processes of a structural evolution from the parent phases toward the intergrowth phase. Systematic evaluation of various types of newly observed and defined growth faults leads to a reorganization model based on the creation of intermediate melts and insufficient dissolution of parent structures. This study provides a different angle to correlate the structural chemistry and the synthesis process in a new approach.

Experimental

A series of *i*BTN ceramic samples were obtained by a two-step processing: a solid-state pre-reaction synthesis and a subsequent reactive sintering. Appropriate amounts of high purity Bi_2O_3 (99.9%), TiO_2 (99%), and Nb_2O_5 (99.5%) powders were mixed and then calcined at 900 °C for 7 h; 2 mol% excess of Bi_2O_3 was added to compensate for later volatilization during sintering. The ceramic samples were sintered for 2 h in air at 1050, 1080, 1100, 1120, and 1150 °C, respectively, in a covered Al_2O_3 crucible (hence abbreviated as *i*BTN-1050, *i*BTN-1080, …*i*BTN-1150) after pressing the calcined powders into pellets, and finally reached 96.5–98.8% of the theoretical density at low to high sintering temperatures. More details of processing can be found in Ref. [14].

The powder XRD patterns of these materials were obtained in an X-ray diffractometer (Model D/max-2550 V, Rigaku, Japan). Microstructure observation was performed on the polished surfaces in the back-scattered electron (BSE) mode in a scanning electron microscopy (SEM, Model JSM-5800, JOEL, Japan) equipped with an energy dispersive X-ray spectroscopy (EDXS) system. TEM specimens were prepared by ion-milling (Model 600, Gatan, USA) after polishing and dimpling. Two electron microscopes operated at 200 kV (JEM-2010/2010F, JOEL, Japan) were employed for the TEM, HRTEM, and analytical TEM studies. The high angular annular dark-field (HAADF) observation was performed in the microscope with a field-emission gun and equipped with a scanning unit.

Results and discussion

Phases and microstructures

The X-ray powder diffraction (XRD) patterns in Fig. 1a show that pre-reaction synthesis at 900 °C produced only the parent BTN ($m = 2$) and BiT ($m = 3$) phases. The *i*BTN phase ($m = 2 + 3$) was formed through reactive-sintering only at higher temperatures according to the following reaction:

$$Bi_3TiNbO_9 + Bi_4Ti_3O_{12} \rightarrow Bi_7Ti_4NbO_{21} \quad (1)$$

The evolution of BTN, BiT, and *i*BTN phases was monitored via the characteristic peaks in the range of 29–30°. All the three phases can be distinguished clearly in the sample sintered at 1050 °C (*i*BTN-1050), for the samples sintered at 1080 °C and above, the *i*BTN phase starts to overwhelm the others. With the increase of sintering temperature, the amounts of BTN and BiT phases decrease at different rates: the BTN phase disappeared at 1100 °C while the BiT phase almost disappeared at 1150 °C.

Besides the parent and intergrowth phases detected by XRD, an additional intergranular phase was also revealed with a bright contrast by back-scattered electron (BSE) imaging in scanning electron microscopy (SEM) as illustrated in *i*BTN-1120 (Fig. 1b). Energy-dispersive X-ray spectroscopy (EDXS) analysis showed that these intergranular regions were enriched in Bi as compared to the main *i*BTN phase. The strong decrease of Ti content relative to Bi could not be due to the remaining secondary phase BiT since it has a higher Ti content as the matrix, while BTN phase was no longer present for the samples sintered above 1100 °C.

The microstructure evolution in this series of *i*BTN ceramics reveals a trend toward anisotropic grain growth, which can be divided into two stages with low and high sintering temperatures. Bright-field (BF) TEM images from

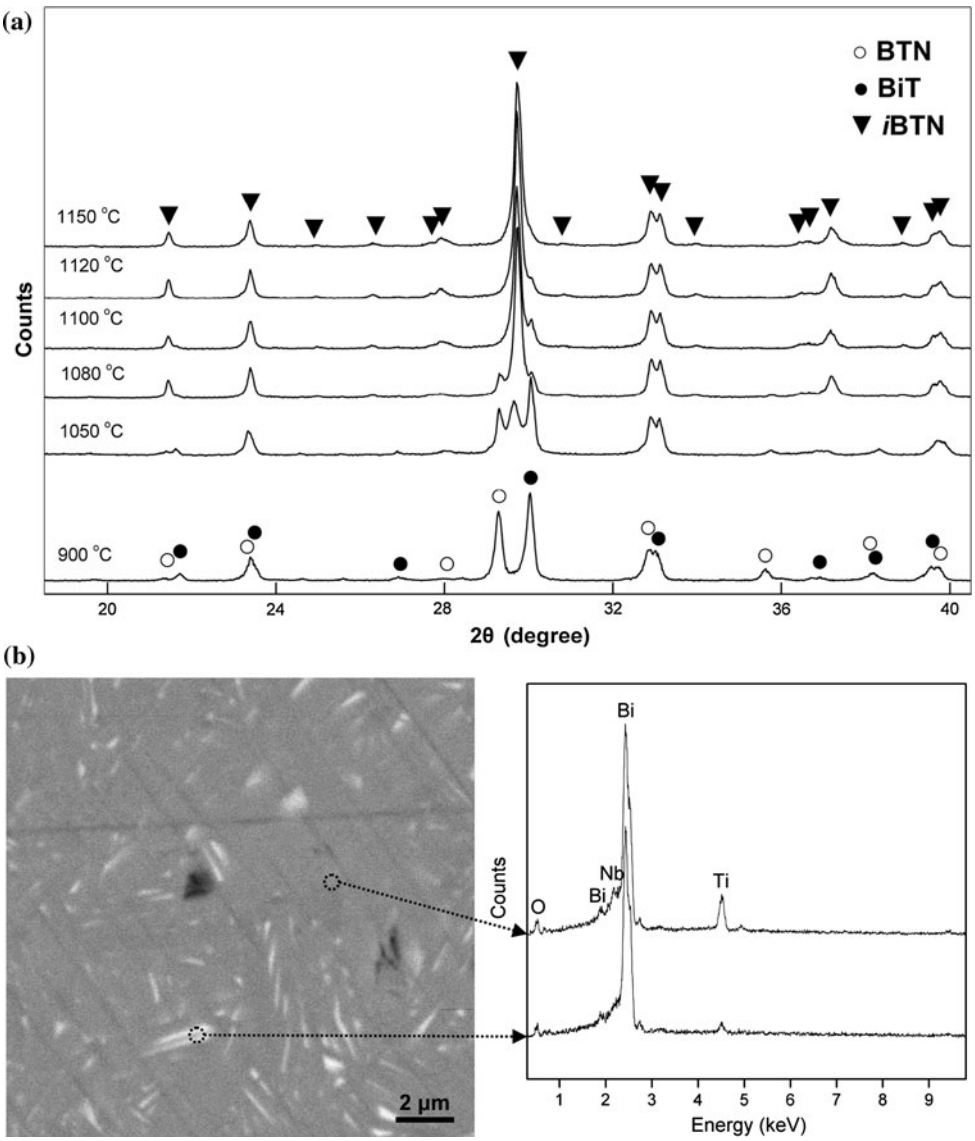

Fig. 1 **a** XRD patterns of the *i*BTN samples reactive sintered at the temperatures between 1050–1150 °C; the two starting phases were calcined at 900 °C as also presented here. **b** An unknown intergranular phase as revealed by the bright contrast in BSE image of *i*BTN-1120 (left); the accompanying EDXS spectra indicating that this is neither BTN nor BiT phases. See text for more details (right)

*i*BTN-1050 and *i*BTN-1080 samples exhibit usually large and elongated *i*BTN grains mixed with smaller and equi-axed BTN/BiT grains, as shown in Fig. 2a. Contrarily, the samples sintered between 1100 and 1150 °C exhibited a microstructure with fully anisotropic grains for the *i*BTN phase (Fig. 2b). In the first stage of *i*BTN grain growth (1050–1080 °C), many small BTN and BiT grains still remained within the microstructure while the aspect-ratio of large *i*BTN grains is generally between 2 and 4, indicating a moderate anisotropic grain growth. In the second stage of 1100–1150 °C, much fewer BiT grains were present while the elongated *i*BTN grains have the aspect-ratio well above five and many even reaching ten, revealing a strong anisotropic grain growth. To identify the BTN, BiT, and *i*BTN phases in TEM, especially in the first stage, the EDXS analysis was employed by comparing the relative intensities of Nb-*L* and Nb-*K* peaks to the Ti–*K* peaks (Fig. 2c).

Ordered intergrowth and growth faults

The ordered stacking sequences (2·3) of the constituent BTN ($m = 2$) and BiT ($m = 3$) unit layers in *i*BTN ($m = 2 + 3$) intergrowth structure can be directly visualized by the HRTEM observation along the [010] zone-axis, as shown in the left image in Fig. 3a. In addition, high-resolution high-angle annular dark-field (HAADF) image can directly visualize heavier Bi atoms positions in the intergrowth structure (the right side of Fig. 3a), which exhibit an excellent match with the reported *i*BTN structure [11].

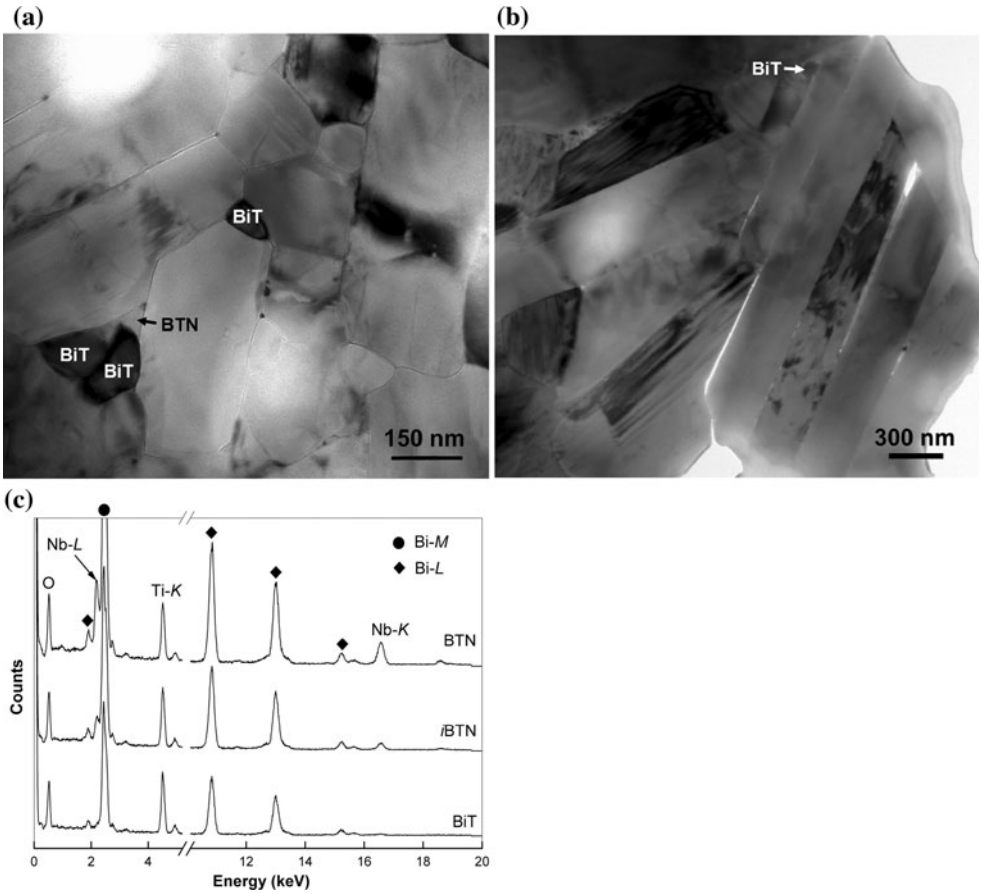

Fig. 2 The BF images exhibit the typical microstructure of *i*BTN-1080 (**a**) and 1120 (**b**). The EDXS spectra of the BTN, BiT, and *i*BTN phases are shown in (**c**)

However, local continuous sequences of "-BiT-BiT-" (3·3) in the ordered (2·3) stacking sequence of *i*BTN structure could be frequently observed by HRTEM. As shown in Fig. 3b, one or two extra BiT layer(s) were inserted into the *i*BTN lattice to form single or double stacking faults, as indicated by the single or double arrows, respectively. Similar single and double faults formed by the extra inserted BTN layer(s) in *i*BTN were more frequently found to form (2·2) sequences, as shown in Fig. 3c. Such stacking faults occur more often in the samples sintered at relatively lower temperatures, especially in *i*BTN-1050 and *i*BTN-1080, while single BTN and BiT faults could also be found in *i*BTN-1150 but in much less frequency. Furthermore, the triple BTN faults could also be observed, but only in *i*BTN-1050. It is worth noting that the evenly spaced single BTN or BiT faults may also be regarded as new stacking sequences of (2·2·3) and (3·3·2), respectively; one case is shown in Fig. 3c. These new stacking orders could also be taken as new intergrowths of $Bi_{10}Ti_5Nb_2O_{30}$ ($m = 2 + 2 + 3$) and $Bi_{11}Ti_7NbO_{33}$ ($m = 3 + 3 + 2$) within the matrix of (2·3) sequence.

In parallel, mono-layers of BTN were also observed in the BiT lattice in *i*BTN-1100 as shown in Fig. 3d, while BiT mono-layer was never found in BTN structure. This indicates that the BiT structure could also host layered growth faults similar to the intergrowth phase, although they could not be taken as the stacking faults since these layered faults are constituted of non-constituent layers. Furthermore, thin ribbons of alternative (2·3) stacking sequences could also be found on the surface of BiT grains, hence forming local *i*BTN phase, as shown in Fig. 4a. Such co-existence of *i*BTN and BiT structures was often observed in *i*BTN-1050 and *i*BTN-1080, and can be regarded as a "co-growth" structure to distinguish from the intergrowth, which is characterized by a coherent intra-granular boundary as marked by the white line in Fig. 4a, indicating that it should be formed via the epitaxial growth onto BiT grain along the common [001] directions. The *i*BTN co-growth was always grown adjacent to a BTN grain, or sandwiched between BiT and BTN grains, as revealed in Fig. 4b. Similar co-growth of *i*BTN on BTN grain was never found.

The "elastic force" model for intergrowth is based on the competition of strain energies induced by the lattice mismatch between the $[Bi_2O_2]^{2+}$ layers and various perovskite-like layers [15, 16]. The presence of a variety of

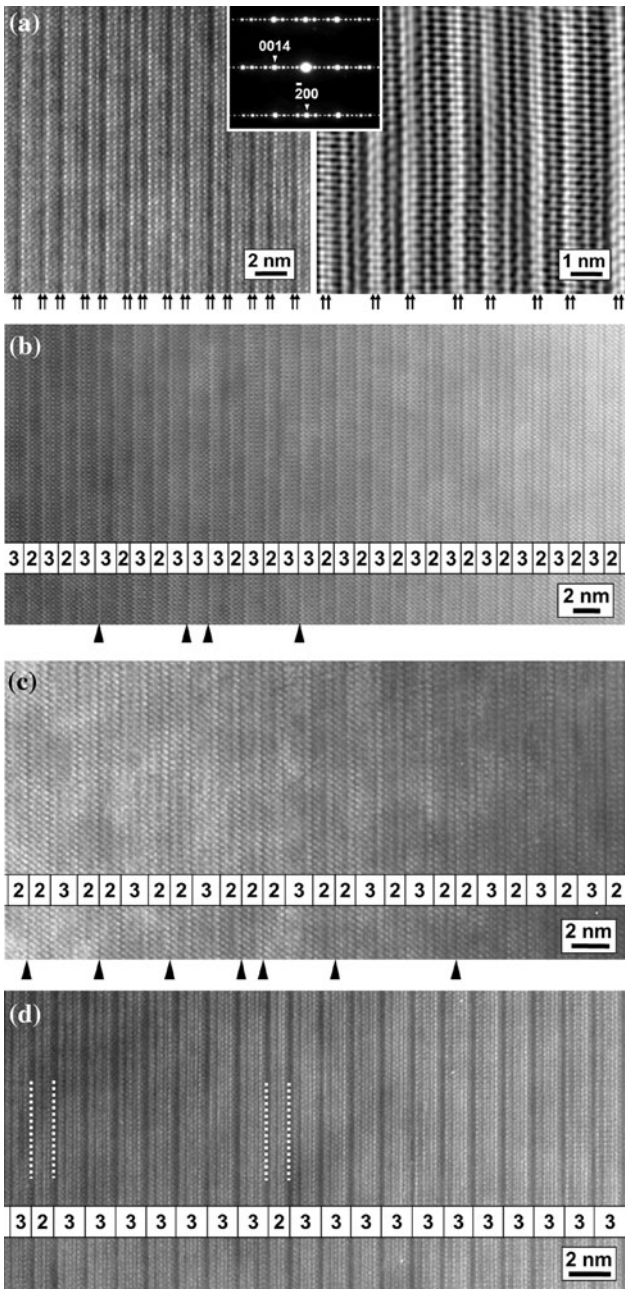

Fig. 3 **a** HRTEM (left) and HAADF (right) images of the *i*BTN structure along the [010] zone axis (insert: SAED pattern), the $[Bi_2O_2]^{2+}$ layers are labeled by dark double-arrows. **b** and **c** are typical BiT and BTN stacking faults respectively in *i*BTN structure along the [110] zone axis, as marked by dark arrows. **d** BTN-layered faults in BiT lattice along the [100] zone axis as labeled by white dotted lines

different stacking sequences in the intergrowth lattice would constitute a complex situation for local strain competition under this picture unless other factors dominating. In fact, all these different faulted structures, including stacking fault, layered fault, and co-growth, were various types of growth faults created within or together with the

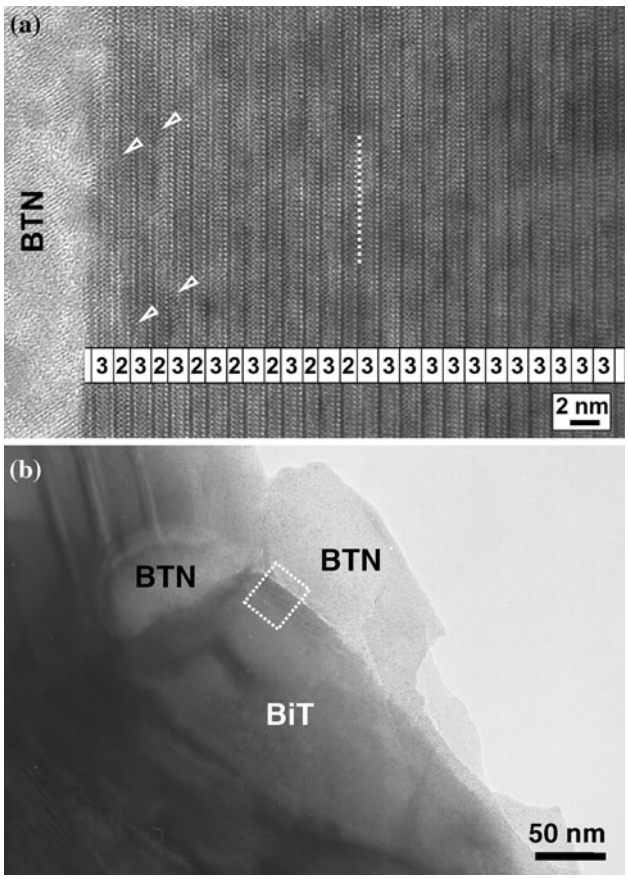

Fig. 4 **a** HRTEM image of *i*BTN-BiT co-growth structure along the [110] zone axis in *i*BTN-1080 with the intra-grain phase boundary marked by the white line, as taken from the box region in **b**; step-like defects are marked by arrows. **b** BF image of the BiT-*i*BTN co-growth structure in *i*BTN-1100

intergrowth structure, hence could not be interpreted from the strain energy alone. Therefore, in the following sections, we will propose a different model to explain collectively the formation of intergrowth structures and the associated various types of growth faults.

Solution—precipitation process

The formation of intergrowth structure was witnessed and accompanied by the creation of various growth faults during the reactive-sintering process. The XRD patterns in Fig. 1 indicate that the transformation from BTN and BiT phases into *i*BTN phase was a gradual process and can be completed till temperatures approaching 1150 °C. The epitaxial growth of *i*BTN on BiT indicates that the confined *i*BTN structure was created via heterogeneous nucleation to form a "core–shell" structure, which suggests a local process via solution-precipitation mode [20, 21]. In other words, the co-growth *i*BTN layer has grown out from the local intergranular melt as a result of partial dissolution of

BTN and BiT grains. Otherwise, it is difficult to imagine a diffusion path for BTN to enter directly and deeply into the BiT lattice without severely modifying or even destroying the native structure. Indeed, co-growth of *i*BTN usually occurred on a relatively large BiT grain among an agglomerated cluster of remaining BTN grains, as shown in Fig. 5a, which indicates that these residual BTN grains were survived from the dissolution process while collected by the flow of melts. The remaining BiT grains were relatively larger to facilitate the epitaxial growth of the local *i*BTN co-growth from the melts. In this regard, residual BTN and BiT grains due to partial dissolution should correspond to the incomplete reaction at 1050 °C and 1080 °C revealed by the XRD result (Fig. 1).

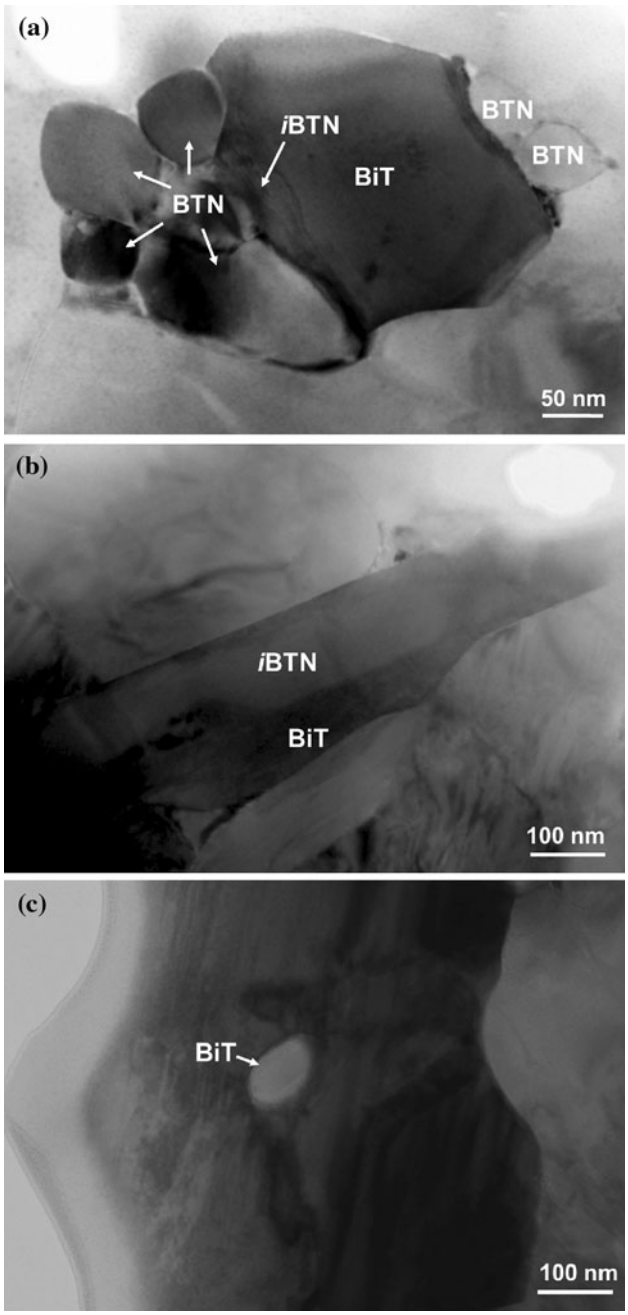

Fig. 5 BF images of **a** an *i*BTN co-growth structure in a BiT grain among a cluster of agglomerated BTN grains in *i*BTN-1050; and **b** a BiT co-growth structure grown onto an elongated *i*BTN grain in *i*BTN-1100; **c** Intra-granular BiT grain residual from dissolution to remain inside the growing *i*BTN phase, in a BF image of *i*BTN-1100

The main intergrowth phase should also be created from similar solution-precipitation processes during the reactive sintering. In contrast to the co-growth structure, the normal *i*BTN grains were formed via homogeneous nucleation, while the melts created from dissolution could facilitate the *i*BTN phase to grow all in elongated grains. At relatively low sintering temperature, the dissolution was rather slow to form relatively less melts, hence to achieve moderate aspect-ratios for the elongated grains (Fig. 2a). The faster dissolution at elevated temperatures should increase the rates of dissolution and anisotropic growth to reach the higher aspect-ratios for *i*BTN grains (Fig. 2b). In a normal solid-state reaction via most probably the evaporation–condensation process rather than the solid diffuse process, a high vapor pressure is required and maintained, which would favor a fast and equiaxed grain growth mode. Furthermore, closing up the pores with high pressure vapor would be rather slow and difficult, which should also be quite sensitive to the reaction temperature. However, the sample sintered even at the lowest temperature had reached a rather good density (96.5% to the theoretical value), indicating that the pore closure was relatively easy during sintering, which was most probable via the dissolved melts that favor the anisotropic growth mode.

In samples sintered at higher temperatures, i.e., *i*BTN-1100/1120/1150, we have observed another type of co-growth of BiT phase on *i*BTN structure, as demonstrated in Fig. 5b. This co-growth forms the same intra-grain boundary as the *i*BTN co-growth (Fig. 4a) via a similar precipitation process, but with an opposite epitaxial relation. In another words, this BiT co-growth was created onto the elongated *i*BTN grains *after* the completion of the formation of intergrowth structure, which is actually a final re-precipitation of BiT phase from the remaining melts. Therefore, the detected BiT phase at higher sintering temperatures by XRD should correspond mainly to such co-growth structures via re-precipitation. The small and round-shaped residual BiT grains can still be found even inside the elongated *i*BTN grains, as shown in Fig. 5c, where the dissolution of BiT was stopped by the start of *i*BTN precipitation. The presence of residual, elongated, and re-precipitated grains at relatively high temperatures should correspond to an extensive process of solution-precipitation and correlated with relatively large amount of melts. Some of the melts even survived the precipitation stage to remain as the Bi-rich phase in the intergranular

regions (Fig. 1b), which will be reported in a separate study later. Such a variety of phase and microstructure features demonstrate that the reaction in Eq. 1 could not fully account for what occurred at the microscopic level even at high temperatures.

Reorganization of nano-layers

In light of the ubiquitous presence of intergranular melts in the formation of different types of growth faults as well as the anisotropic grain growth mode for *i*BTN structure, we present here a reorganization model to rationalize the creation of intergrowth structure together with the associated stacking-faults via an unified solution-precipitation process, based on the difference in the dissolution rates of layered structural units.

The abundant stacking faults in the intergrowth structure should be created in the same solution-precipitation process. Indeed, their numbers in different samples exhibit common trends with sintering temperatures, as summarized in Fig. 6. The numbers of BTN/BiT double-faults decreased down to vanishing at higher sintering temperature, while the triple-faults could no longer be detected even at the intermediate temperature of 1100 °C. At low temperature the numbers of triple-faults were less than the double-ones, which were further less than single-faults. In addition, the frequency to find each type of BTN faults was always higher than the corresponding BiT faults in every case. Since the single-, double-, and triple-faults are formed by 2, 3, and 4 consecutive BTN or BiT layers, and each BTN layer is also thinner than a BiT layer, all the data in Fig. 6 can be combined in an unified trend of decreasing

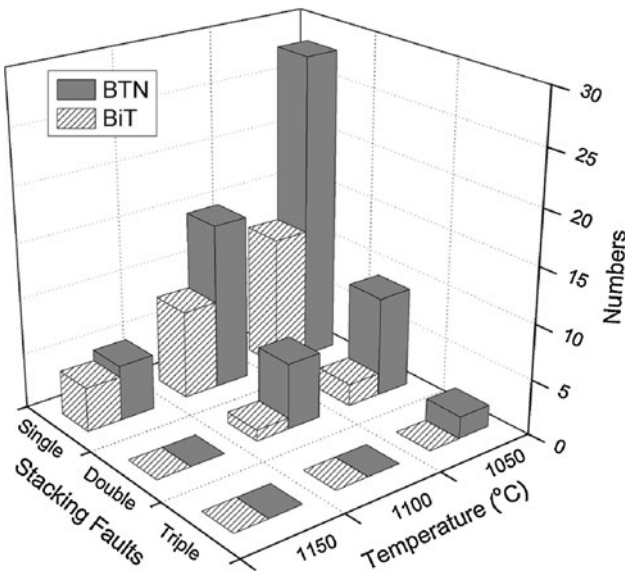

Fig. 6 Frequency of several types of BTN/BiT stacking faults found in *i*BTN grains at various sintering temperatures. About 30 grains were observed by TEM in each material

population either with thicker layers or with increasing temperatures, which follow a common dissolution process. In consequence, all these faults were in fact remnants of the starting BTN and BiT structures that survived the dissolution stage to be retained as the corresponding stacking faults through precipitation.

In the same dissolution process, the even thinner remnants of one-layered BTN and BiT should be more or much more popular than these thicker remnants in all cases, and these populations should also decrease with increasing temperature. In other words, the alternative stacking in this intergrowth structure was created from these one-layered BTN and BiT remnants, leaving the thicker remnants to be retained as the imbedded stacking faults via the common precipitation process. The high aspect-ratio of *i*BTN grains is consistent with the existence of such mono- and multi-layered remnants as in situ templates for nucleation and growth from the melts. The presence of BTN layered faults deep into the BiT lattice (Fig. 3d) is another case of such one-layered structures to remain "intact" through the whole solution-precipitation process.

To nucleate the intergrowth structure from the layered BTN and BiT units (remnants), a self-ordering or reorganizing process should occur to turn from their further dissolution into precipitation. The nucleation of *i*BTN phase directly from the melts is very unlikely because this would enable the formation of both BTN and BiT stacking faults in the same grain, which we have *never* observed. In our model of re-ordering BTN and BiT layered-units in the melts, sufficient inter-diffusion between the two layered-units is required during dissolution before reaching a critical ratio or number to start precipitation. The interfacial force between the two types of layered-units is a critical factor: The dissolution process may develop an attractive interaction between the BTN and BiT layered-units as compared to the same types of layered-units. Such a special solution–precipitation process according to this reorganization model is schematically demonstrated in Fig. 7.

Indeed, the poorly bonded $[Bi_2O_2]^{2+}$ sheets in both the mica-like Aurivillius BTN and BiT structures were preferentially dissolved than the relatively well-bonded Ti-O_6/Nb-O_6 octahedrons in the perovskite blocks [11, 22]. Such a difference allows the melts to have a much higher concentration of Bi cations as compared to Ti and Nb cations. This suggests that the dissolution process may involve an internal melting mode to piece off the layered structure through the $[Bi_2O_2]^{2+}$ sheets, in addition to the normal mode via particle surface. In fact, such exfoliated BTN/BiT layered-units would continue to dissolve into the Bi-rich melts from their edges or severely bending ridges. To start the precipitation, the melts should reach a certain amount to let immerse a critical density of partially dissolved, inter-mixed, exfoliated perovskite sheets, to favor

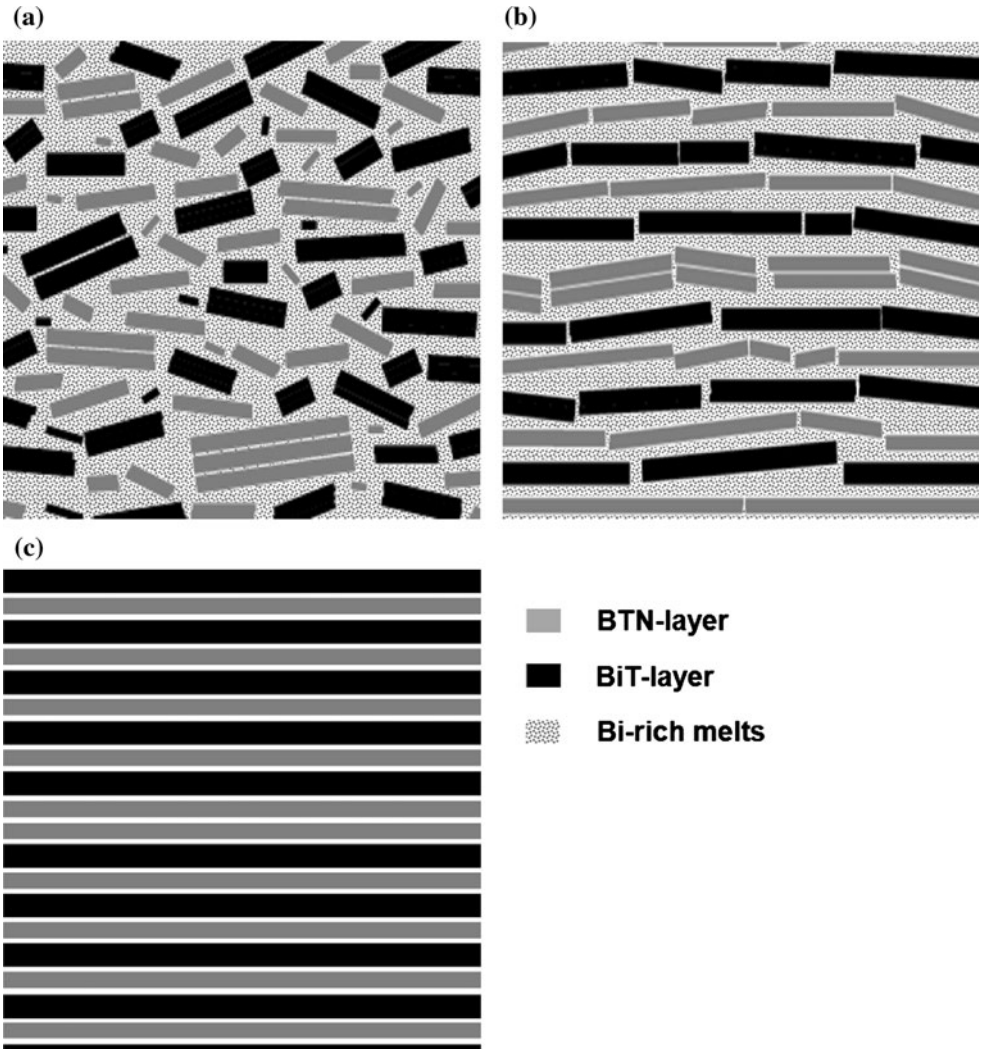

Fig. 7 Schematic illustration of the re-organization process of mainly mono-layered BTN and BiT nano-units (together with some double-, triple-layered units) to form the *i*BTN intergrowth and associated stacking faults: **a** dissolution, **b** re-ordering and **c** final *i*BTN lattice

an attractive force developed at the interfaces between different nano-sheets. Such a reorganization process is distinctive in category with the conventional reprecipitation of a same structure and the precipitation of a completely different structure. It is something between the two "extremes" by re-ordering the same layered-units of two parent structures into an unified structure.

This reorganization model appears quite similar to the alternative mono-layer assembly model for other layered perovskite structures that were created via colloidal routes [23], although in our case the process is promoted by heat without any chemical manipulation, hence the origin of attractive forces should also be quite different. In other words, the exfoliated BTN/BiT layers were formed in situ as nano-templates in the melts. In fact, this is a structural evolution to transform the two layered parent structures into a new structure of intergrowth by retaining the perovskite skeletons while recovering the inter-layered structure.

Such an evolutional process can be naturally extended to interpret the origin of other growth faults such as the layered faults and co-growths, and could also rationalize more complicate intergrowth phenomena reported by Boullay et al., who always found the same *i*BTN intergrowth (2·3) to mix locally with other intergrowths by varying the molar ratio of parent phases [24]. The persistent, hence independent, occurrence of this (2·3) intergrowth (*i*BTN) should be originated from a similar reorganization process even when different intergrowths were expected with strong disparity in BTN and BiT ratios. In other words, the construction of different intergrowths from the parent materials are independent to compositional designing in the macroscopic level, at least via the "solid-state" reactive sintering processes similar to the present case [16, 24, 25]. Future applications of this model to other intergrowth systems are expected.

Conclusions

The reactive sintering to create intergrowth phase of *i*BTN from the parent BTN and BiT phases was found

accompanied by a variety of structure and microstructure features. Based on a systematic analysis on the population of various growth faults and their trends with sintering temperatures, a structural reorganization model emerged from a common solution–precipitation process to interpret the creation of intergrowth structure. The preferential dissolution of the poorly-bonded interleaved $[Bi_2O_2]^{2+}$ sheets enabled the initiation of Bi-rich melts to exfoliate the BTN and BiT layered-units, which were re-ordered into the intergrowth during precipitation together with all types of growth faults. This model refines and re-defines the solid-state reaction to construct the intergrowth as an evolution process that is largely insensitive to the compositional designing at the macroscopic level.

Such a model and rationalization is based on the new findings of: (a) various types of BTN and BiT stacking faults in intergrowth structure, and some may even form locally new intergrowth; (b) the co-growths of *i*BTN on BiT and BiT on *i*BTN at low and high sintering temperatures; (c) the correlation of anisotropic *i*BTN growth with a Bi-rich intergranular phase.

Acknowledgements The authors acknowledge the financial support from the Chinese National Natural Science Foundation (Grant No. 50932007) and the Ministry of Science and Technology of China through 973-Project (Grant No. 2009CB613305), as well as the travel support from the bilateral cooperative research program between China and Slovenia (project No. 07-06). The authors also wish to thank Drs. Xianhao Wang, Juanjuan Xing, and Sašo Šturm for helpful discussions.

References

1. Park BH, Kang BS, Bu SD, Noh TW, Lee J, Jo W (1999) Nature 401:682
2. de Araujo CAP, Cuchiaro JD, Mcmillan LD, Scott MC, Scott JF (1995) Nature 374:627
3. Aurivillius B (1949) Ark Kemi 1:463
4. Frit B, Mercurio JP (1992) J Alloys Compd 188:27
5. Noguchi Y, Miyayama M, Kudo T (2000) Appl Phys Lett 77:3639
6. Goshima Y, Noguchi Y, Miyayama M (2002) Appl Phys Lett 81:2226
7. Shibuya A, Noda M, Okuyama M, Fujisawa H, Shimizu M (2003) Appl Phys Lett 82:784
8. Kikuchi T (1976) J Less Common Met 48:319
9. Kikuchi T, Watanabe A, Uchida K (1977) Mater Res Bull 12:299
10. Maalal R, Mercurio D, Trolliard G, Mercurio JP (1998) Ann Chim Sci Mat 23:247
11. Mercurio D, Trolliard G, Hansen T, Mercurio JP (2000) Int J Inorg Mater 2:397
12. Boullay Ph, Mercurio D (2004) Integr Ferroelectr 62:149
13. Zhang LN, Li GR, Zhao SC, Zheng LY, Yin QR (2005) Key Eng Mater 255:280
14. Yi ZG, Wang Y, Li YX, Yin QR (2006) J Appl Phys 99:114101
15. Rao CNR, Thomas JM (1985) Acc Chem Res 18:113
16. Rao CNR (1985) Bull Mater Sci 7:155
17. Horiuchi S, Kikuchi T, Goto M (1977) Acta Cryst 33:701
18. Chu F, Damjanovic D, Steiner O, Setter N (1995) J Am Ceram Soc 78:3142
19. Subbanna GN, Ganapathi L (1987) Bull Mater Sci 9:29
20. Hu JF, Gu H, Chen ZM, Tan SH, Jiang DL, Rühle M (2007) Acta Mater 55:5666
21. Xing JJ, Gu H, Gloter A, Shen H, Pan XM, Wang PC (2007) Acta Mater 55:5323
22. Poterala SF, Chang Y, Clark T, Meyer RJ Jr, Messing GL (2010) Chem Mater 22:2061
23. Schaak RE, Mallouk TE (2002) Chem Mater 14:1455
24. Boullay Ph, Trolliard G, Mercurio D, Perez-Mato JM, Elcoro L (2002) J Solid State Chem 164:252
25. Sagalowicz L, Chu F, Martin PD, Damjanovic D (2000) J Appl Phys 88:7258